One same initiating molecule and two divided downstream pathways? — Mechanism of aluminum-induced programmed neural cell necrosis

Yan-xia Hao
Shanxi Medical University
Jin-tao zhang
Shanxi Medical University
Jing-si Zhang
Shanxi Medical University
Huan Li
Shanxi Medical University
Chan-ting He
Shanxi Medical University
Shu-hui zhang
Shanxi Medical University
Shan Wang
Shanxi Medical University
Yue Zhou
Shanxi Medical University
Qiao Niu (niuqiao55@163.com)
Shanxi Medical University

Research Article

Keywords: aluminum, necroptosis, RIP3, MLKL, CaMK

Posted Date: May 9th, 2022

DOI: https://doi.org/10.21203/rs.3.rs-1614222/v1

Abstract

Objective

The research is to elucidate the mechanism of programmed neuronal necrosis induced by aluminum exposure. The mechanism of programmed neuronal cell necrosis caused by aluminum exposure is due to the key death proteins RIP1, RIP3, MLKL and CaMK□ in vivo and vitro experiments.

Methods

In vivo study, mice were intraperitoneally injected with freshly prepared maltol aluminum for two months to establish aluminum-induced cognitive impairment model. The key death related proteins were measured by Western blot and the relationships between those proteins were detected by IP. LDH release was used to show the cell death, and ROS indicated the damage of brain. In Al-exposed SH-SY5Y cells, GSK'872 was interfered to observe the expression of key death related proteins by WB and IP, as well as PI dyeing. Besides, NSA and KN-93 were administered to detect the LDH release and ROS change, including mitochondrial membrane potential variation in the Al-exposed cells.

Results

Expression of RIP1, RIP3, MLKL and CaMK□ proteins were increased in vivo and vitro study after aluminum exposure. Inhibition of RIP3, MLKL and CaMK□ protein expression could reduce PI stained cells and LDH release. ROS declined after administration of GSK'872 and NSA in Al-exposed cells, while mitochondrial membrane potential elevated after intervention of KN-93 in Al-exposed cells with decreased mitochondrial membrane potential.

Conclusion

Programmed neuronal necrosis was one of the main causes though that aluminum lead to neuron reduction. The signal pathways involved in programmed necrosis were RIP1-RIP3-MLKL and RIP1-RIP3-CaMK□ pathways, one same initiating molecule – RIP1, two downstream pathways: RIP3-MLKL pathway and RIP3-CaMKII pathway.

Introduction

Aluminium, as the third most abundant metal element on earth, is widely used in construction, aviation, papermaking, pharmacy, cosmetics, food industry, water treatment system (Dabeka, Fouquet, Belisle, & Turcotte, 2011; Tomljenovic & Shaw, 2011). In our surrounding environment, we seem to inevitably contact with aluminum everywhere. Aluminium, while plays an important role in our life, also poses a certain threat to humans' health, which is mainly manifested in its toxicity on the nervous system

(Hanninen, Matikainen, Kovala, Valkonen, & Riihimaki, 1994). Epidemiological evidence confirmed that people with higher levels of aluminium in drinking water had a higher risk of dementia than those who also drank relatively low levels of aluminium (Russ et al., 2019). Aluminum can lead to cognitive dysfunction among workers employed in occupational aluminum exposure environment (Meyer-Baron, Schäper, Knapp, & van Thriel, 2007), and also affects the impairment of visual spatial function, especially the recognition of spatial location(S. Wang et al., 2020). Cognitive dysfunction caused by aluminum has been confirmed in human and in vivo and in vitro experiments(Bondy, 2010). There is some evidence supporting neurotoxic effects of aluminium in terms of generating reactive oxygen species (ROS) (Han et al., 2013), decreased synaptic plasticity(Liang et al., 2012), inducing neurofibrillary tangles(Edwardson et al., 1992; J. Nie, 2018), accumulation of β-amyloid (Aβ)(Kawahara & Kato-Negishi, 2011), mitochondrial metabolism dysfunction(Jisheng Nie, Lv, Fu, & Niu, 2019), neuroinflammation(Z. Cao et al., 2016), loss of neuronal cell including cell apoptosis(Prakash & Kumar, 2013), and non-apoptotic regulated cell necrosis(Qinli et al., 2013).

Necroptosis, a form of non-apoptotic regulated cell necrosis, traditionally considered to be a passive cell death, which can be performed through precise cellular signaling pathways(Degterev et al., 2005). Typical necrotic morphology are the death features of necroptotic cells, including early plasma membrane permeability, organelle swelling, nuclear membrane dilation, and chromatin concentration(Vandenabeele, Galluzzi, Vanden Berghe, & Kroemer, 2010). Eventually it ends with the rupture of the cell membrane and the cell contents are released, often leading to inflammation(Ofengeim & Yuan, 2013). Receptor interacting protein 1 (RIP1) and receptor interacting protein 3 (RIP3) play key roles in necroptosis. When RIP1 is activated, it can bind and activate RIP3 through RHIM, and the two form a large necrosom to initiate necroptosis(J. Li et al., 2012). MLKL, which is a downstream substrate of RIP3, being activated by RIP3, then is transformed from a monomer state to a multimer state and forming a permeable pore in the cell membrane, destroying the cell membrane and causing cell death in the ending(H. Wang et al., 2014). Recently, CaMKII was found to be another substrate of RIPK3, which plays an important role in programmed cell death during myocardial ischemia(T. Zhang, Zhang, & Cui, 2016). CaMKII is activated by direct phosphorylation and indirect oxidation, which leads to the opening of mitochondrial nuclear membrane pores, and finally leads to cell death after the decrease of mitochondrial membrane potential(T. Zhang et al., 2016). CaMKII is abundantly present in the central nervous system(Ishida, Shigeri, Taniguchi, & Kameshita, 2003). It is reported that CaMK□-δ is phosphorylated by RIPK3, and p-CaMK□-δ leads to oligodendrocytes necroptosis in the developing brain(Qu et al., 2017). Our research group has proved that there is a phenomenon of nerve cell loss in the aluminum-induced dementia model, and the death pathways include apoptosis, programmed necrosis, and autophagy(Qinli et al., 2013). RIPK1 (receptor interacting protein, RIP1) plays an important role in the process of aluminum-induced neuronal programmed necrosis(Hao et al., 2020). RIPK1 activated its downstream RIPK3 to trigger the programmed necrosis process, but different studies have found different signaling molecular pathways downstream of RIPK3 in different tissues. Which one downstream molecule and its pathway the aluminum-induced neuronal necroptosis is? Is it MLKL or CaMKII? or both? This research explored the key molecules downstream of RIPK3 in the signaling pathway of neuronal programmed necrosis caused

by aluminum, and provided a theoretical basis for elucidating the mechanism and possible target for invention of cognitive impairment in aluminum-induced dementia model.

Materials And Methods

Maltoaluminum preparation The formulation of the aluminum maltol mixture has been described in previous report (Song, Liu, Zhang, & Niu, 2016). $AlCl_3$·6H2O (Sigma Chemical Co, MO, USA) was dissolved in distilled water to a final concentration of 20 mM. Maltolate (Sigma Chemical Co, MO, USA) was dissolved in phosphate buffered saline (PBS) until the final concentration was 60mM. The two solutions were mixed in equal volumes to make a final concentration of 10 mM $Al(mal)_3$, then adjusting the mixture pH 7.4 with 10% NaOH, and filtering impurities through a 0.22 μl filter finally. $Al(mal)_3$ was freshly prepared for each study process.

Animals The experimental mice were provided by the animal experiment center of Shanxi Medical University, and the research was approved by the Ethics Committee on Experimental Animals at Shanxi Medical University. C57BL/6 mice weighing 20-25g, aged 8 weeks, were fed with the same feed and drinking water freely and each mouse was reared in a single cage under constant humidity and temperature with a 12-h light/dark cycle.

Aluminum-induced dementia model

The mice were randomly divided into four groups (n = 8 per group): control group, three $Al(mal)_3$ administration groups. In $Al(mal)_3$ treatment group, the mice were administrated with an intraperitoneal injection of $Al(mal)_3$ at dose of 20μmol•kg^{-1}, 40μmol•kg^{-1}、80μmol•kg^{-1} for two months. The control mice were injected with normal saline according to mice weight. Each injection was conducted for consecutive 5 days and was paused for 2 days.

Behavioral tests for learning and memory

Morris water maze (MWM)

The experimental device was a circular pool with a height of 45 cm and a diameter of 100 cm. The pool was divided into 4 quadrants according to the marked east, west, south and north positions on the inner wall of the pool, and the platform submerged 0.5–1 cm below the water surface was placed in the target quadrant. One day before the start of the experiment, each mouse was allowed to swim for 60 s to adapt to the environment. Positioning navigation training test was conducted 5 days before the formal experiment to record the time from the mouse entering the water to finding the platform. If the mouse did not found the platform within 60 seconds, the mouse was guided to the platform and stayed on it for 10s. On the sixth day for space exploration experiment, the platform in the pool was evacuated, and the number of times the mouse crossed the platform within 60 seconds was recorded.

Novel Object Recognition Task

The new object recognition test was a learning and memory test method based on that rodents have an innate preference for novelty to assess cognitive changes, especially short-term memory ability, in animal models of neurodegenerative diseases(Foyet & Keugong Wado, 2019). The day before the test, the mouse was placed in an empty 40×40×40cm^3 box and allowed to explore freely for 5 minutes. On the day of the test, two identical cubes A and B were stably placed in the box. The edge of the cubes was 5cm away from the two adjacent side walls of the box. The mouse was left to these two identical objects for 10 minutes to let the mouse being familiar with them. After that, the mouse was taken out of the box, remove one of the two identical objects, and randomly replace another new object in place. The color, texture, and shape of the new object were different from the old one, and the mouse was tested in the inner of box for 5 minutes. Etho Vision XT 9 software was used to record the time spent by the mouse to explore each object. The time to explore new objects was recorded as (new, N) and the time to explore familiar objects was recorded as (familiar, F). New object recognition index = N / (N + F) × 100%. Old object recognition index = F / (N + F) × 100%. Discrimination index = (F-N) / (F + N) × 100%(Leger et al., 2013).

Sample Preparation

Killed by decapitation, mice brain was removed quickly on ice. A part of the brain was immediately fixed with 10% neutral formaldehyde for the later stage of paraffin embedding, and another part of the cortex and hippocampus was separated and preserved in refrigerators at -80°C for further study.

Nissl staining of the brain

Paraffin sections were dewaxed to water, staining with thionin for 30 min in a 56°C incubator. Sections were rinsed in running water for 15 seconds, and then were decolorized with 95% ethanol + 1% glacial acetic acid for 1 second. Sections were subsequently dehydrated with an increasing ethanol series (95% and 100%) and xylene and mounted with Micromount mounting medium, and observed under microscope and was photographed.

Electron microscope observation of cell ultrastructure

The fresh hippocampus tissue of the mouse was taken out, and the hippocampus tissue was cut into tissue pieces with a volume ≤ 1 mm^3, then fixed with glutaraldehyde-osmium acid, dehydrated with acetone overnight at 4 ℃. After soaking, embedding, and polymerization, trimming and positioning were performed to make ultra-thin slices. After staining, the specimen was observed with an electron microscope.

Cell necrosis rate and apoptosis rate

The cells in the 6-well plate were digested with trypsin and collected. Then the cells were washed twice with a pre-cooled PBS solution. 1×Binding Buffer working solution was added to the collected cells, and the cells were resuspended to a concentration of 1×106 cell/ml. After that, 200μL of cell suspension was pipetted into a new EP tube, and 5μL Annexin V-FITC and 10μL PI solution were added and mixed gently, and incubated for 20min at room temperature in the dark. After staining and incubation, 400 μL

1×Binding Buffer was added to each tube, and then the mixture was detected by flow cytometry (detected within 1 hour).

Released LDH

The protein samples were quantified by BCA method, and then LDH was measured. During the experiment, blank wells, standard wells, test wells and control wells were set up. Double-distilled water, 0.2μmol / ml pyruvate standard application solution, samples, matrix buffer and Coenzyme Ⅱ application solution were added to 96-well plates. Then the above-mentioned materials were mixed, and bath-warmed at 37 ℃ for 15 minutes. Then 2,4-dinitrophenylhydrazine was added, warmed at 37 ℃ for 15 minutes after mixing solution. Finally, 0.4mol/L NaOH solution was added, mixed and placed at room temperature for 5 minutes. The absorbance value at 450nm was measured with a microplate reader.

ROS

Samples were collected and then washed 2–3 times with PBS. The samples were centrifuged in a high-speed centrifuge at 5000r/min and low temperature for 5min, and the supernatant was discarded. PBS was added and the above-mentioned steps such as centrifugation and cells suspension were repeated once. 20μM DCFH-DA was added to the single cell suspension of each group in the same volume (final concentration is 10mM), and the mixture were incubated in a constant temperature shaker at 37°C for 1h. After 1 hour, the single cell suspension was collected and then centrifuged at 5000 r/min for 5 min, and washed 1–2 times with PBS, and then resuspended for detection. The flow cytometer detected the green fluorescence intensity. The best excitation wavelength is 500 ± 15nm, and the best emission wavelength is 530 ± 20nm.

Mitochondrial membrane potential

The cells in the 6-well plate were digested with trypsin and were collected in EP tube. The cells in each well were suspended in 0.5 mL cell culture medium, and mixed with 0.5 mL JC-1 staining solution and shook up and down for several times. The cells were incubated at 37℃ for 20 min in the incubator. 4mL distilled water was added to each 1mL JC-1 staining buffer (5X) to prepare an appropriate amount of JC-1 staining buffer (1X) and placed in an ice bath. After incubation at 37℃, sample was centrifuged at a speed of 600g at 4℃ for 3–4 min to precipitate the cells and the supernatant was discarded. After washing twice with JC-1 staining buffer (1X) and resuscitating with appropriate amount of JC-1 staining buffer (1X), flow cytometry was used for analysis on cell precipitation.

Western blot analysis

Total proteins of mouse hippocampal tissue were extracted and their concentration were measured using Tissue Protein Extraction Kit (CoWin Biotech Co.,Beijing, China). Each lane loaded equal amounts of protein samples (70 μg) was separated by 8% SDS-PAGE gel and transferred to a polyvinylidene fluoride membrane. After soaking in 5% skimmed milk in PBST for 2h to block nonspecific binding, the membranes were incubated overnight at 4°C with anti-CaMKⅡ antibody (1:4000, Gene Tex, Temecula, CA,

USA), anti-p-CaMKⅡ (1:1000, Thermo Fisher, USA), anti-ox-CaMKⅡ (1:1000,Millipore, Billerica, MA, USA), anti-RIP1 (1:1000, Abcam), anti-RIP3 (1:1000, Abcam), anti-MLKL (1:500, Santa Cruz, CA), anti-p-MLKL (1:1000, Cell Signal Technology), anti-NLRP3 antibody (1:1000, Cell Signal Technology), or mouse β-actin 1: 600 (1:600, CoWin Biotech Co., Beijing, China). After washed three times in PBST for 10 min, the membranes were incubated at 37°C for 1.5 h with a HRP secondary antibody: anti-rabbit IgG (1:3000, CoWin Biotech Co., Beijing, China) or anti-mouse IgG (1:3000, CoWin Biotech Co., Beijing, China). Bands were evaluated by the ECL western blot detection kit (CoWin Biotech Co., Beijing, China) and were analyzed using jetta gel image analysis system.

Immunoprecipitation **(IP)**

RIP3 antibody (1:50, Biovision) was added to 1000ug protein, and shook slowly overnight on a shaker at 4°C. 40ul fully resuspended Protein G/A garose was added, shook slowly on a shaker at 4°C for 4h. The sample was put in a 4°C centrifuge, and centrifuged at 12000 rpm for 5 minutes. The sample was washed 5 times with PBS, and supernatant was discarded after each washing carefully. The pellet was resuspended with 40ul 1×SDS-PAGE electrophoresis loading buffer, and then put into a metal bath at 95°C for 10 minutes. The mixture was centrifuged for 1 minute at 2500 rpm and 4°C before electrophoresis. Western blot analysis was used to analyze RIP1, MLKL, and CaMKⅡ proteins in immune complex samples.

Statistical analysis

Statistical analysis was performed with SPSS 22.0 statistical software package. The measurement data is expressed as mean ± SD. after normality test and homogeneity analysis of variance. One-way analysis of variance was used for comparison of means between multiple groups, and LSD-t method was used for comparison between multiple groups. P value less than 0.05 was considered statistically significant.

Result

Results of animal experiments

Morris Water Maze In the positioning navigation experiment, the escape latency of mice in the control group and the experimental group was gradually shortened with the increase of training days. On the 4th and 5th days of training, the escape latency of mice in the aluminum exposure group was significantly higher than that of the saline control group. At the same time, the escape latency of the 80μmol/kg Al exposure group was significantly higher than that of the 20μmol/kg and 40μmol/kg Al exposure groups, and the difference was statistically significant ($P < 0.05$, Fig. 1a).

In the space exploration experiment, in each aluminum exposure group, the number of times the mice crossed the platform gradually decreased with the increase of the aluminum exposure dose. Compared with the control group, the 40μmol/kg and 80μmol/kg Al groups showed statistical differences ($P < 0.05$,

Fig. 1b). It shows that the spatial memory of mice reduced after aluminum exposure, which proved that aluminum had a detrimental effect on the learning and memory ability of mice.

Object recognition test As the aluminum exposure dose increased, the new object recognition index of mice in each aluminum exposure group was gradually lowered than that of the saline control group ($P < 0.05$). The difference between the low-dose aluminum exposure group and the medium and high-dose aluminum exposure groups was statistically significant ($P < 0.05$), but there was no statistically significant difference between the medium-dose aluminum exposure group and the high-dose aluminum exposure group (Fig. 1c). Figure 1d showed the discrimination index of mice. With the increase of the aluminum exposure dose, the new object discrimination index of each aluminum exposure group showed a gradual decrease compared with the control group ($P < 0.05$). The difference between the low-dose aluminum exposure group and the medium and high-dose aluminum exposure groups was statistically significant ($P < 0.05$), but there was no significant difference between the medium and high-dose aluminum exposure groups ($P > 0.05$). It shows that when the aluminum exposure dose increased, the new object recognition index and the discrimination index of the experimental animals gradually reduced. It means that the mice have forgotten the old objects they have been familiar with after Al-exposure, the mouse's short-term learning and memory function was impaired. However, when the aluminum exposure level got a certain degree, the elevation of adverse effect seemed to be not significant.

Nissl staining In the control group, there were 4 layers of small pyramidal cells distributed in CA1 region. The cells were abundant, arranged closely and orderly, with obvious stratification and complete structure. The large pyramidal cells in CA3 region were closely distributed and there was a large number of neurons. The neurons were large in size and regular in shape. Most of them were conical and spherical, and the cell structure was clear. Nissl bodies were dense, large in number, uniformly dyed, granular and blue-purple stained (Fig. 2A1, A2, A3).

In the aluminum exposure group, the number of small pyramidal cells distributed in the CA1 area decreased, and the intercellular space in some areas increased. The number of large pyramidal cells distributed in the CA3 area reduced, with the loosen distribution, and the arrangement was disordered. The shape of neurons was irregular, and part of the cell body was shrunken. The number of Nissl bodies reduced, and the staining color was light and uneven. With the increase of the dose of aluminum treatment, the appearance of the above-mentioned hippocampal cells gradually increased. (Fig. 2B1-3, C1-3, D1-3)

Electron microscopy In the saline control group, the size and morphology of the neuron cell bodies were normal, elliptical, and the double-layer membrane structure of nucleus was intact and smooth. The nucleolus was large and clear, and the structure was intact. Chromatin is granular and evenly distributed in the nucleus. The structure of organelles in the cytoplasm of nerve cells was complete. The mitochondrial morphology and size were normal, and the mitochondrial cristae were lamellar. (Fig. 3A1, A2)

After administration of aluminum, the cell body of the neuron shrank and became round. The cell membrane of the neuron dissolved and broke with the cell content outflowed. With the increase of the Al dose, the cell membrane destruction gradually aggravated, and the cell content gradually decreased. The nucleus becomes shrank and rounded, with blurred convex and concave membrane, and the chromatin in the nucleus increased and gathered toward the edge, without formation of large coagulation (Fig. 3.B1-2, C1-2, D1-2). The rupture and disintegration of the nuclear membrane of neurons in the medium and high dose groups were observed (Fig. 3.C2, D2). Mitochondria in cytoplasm increased and became round, swelling, and mitochondrial crest fracture decreased. The volume of mitochondria in cytoplasm increased and became round and fracture of mitochondrial crest decreased.

LDH Release Lactate dehydrogenase (LDH) is usually used as a measure of body tissue damage. Compared with the control group, the LDH content of the different aluminum exposure groups showed a gradual increase, but there was no significant difference between the 20μmol/kg Al exposure group and the saline control group ($P > 0.05$). The LDH content of the 40μmol/kg and 80μmol/kg Al exposure groups increased, and the difference was statistically significant compared with the control group ($P < 0.05$). The LDH content of the 40μmol/kg and 80μmol/kg Al exposure groups was higher than that of the low-dose aluminum exposure group ($P < 0.05$). (Fig. 4a)

ROS It is generally believed that abnormally elevated levels of free radicals and excessive oxidative stress in brain tissue are one of the main causes of neuronal damage and degeneration. Free oxygen radicals are also called reactive oxygen species (ROS), which account for about 95% of free radicals. In this study, it was found that the content of ROS in the brain tissue of mice in aluminum exposure groups was higher than that in the control group ($P < 0.05$). With the increase of aluminum load, the amount of ROS gradually increased, and showed a dose-response relationship, the difference was statistically significant ($P < 0.05$). (Fig. 4b)

Death related protein expression The key proteins RIP1, RIP3, and MLKL that play critical roles in programmed necrosis in the hippocampus of mice all increased after aluminum exposure. The RIP1 protein gradually increased with the increase of aluminum load, showing a dose-response relationship. Compared with the control group, RIP3 in the hippocampus increased in all aluminum exposure groups ($P < 0.05$), and the highest expression was found in 40μmol/kg Al exposure group ($P < 0.05$). Compared with the control group, the expression of MLKL showed a gradual increase trend after aluminum exposure ($P < 0.05$), and the increase was most obvious in the 80μmol/kg aluminum exposure group. Compared with the control group, the expression of CaMK□ protein had no significant difference ($P > 0.05$), but the expression of p-CaMK□ (Thr287) increased after aluminum exposure ($P < 0.05$). The expression of p-CaMK□ (Thr287) was the highest in the 80μmol/kg aluminum exposure group ($P < 0.05$), but there was no significant change in the expression of p-CaMK□ in the 20μmol/kg and 40μmol/kg aluminum exposure groups ($P > 0.05$). The expression of ox-CaMK□ did not change significantly after aluminum exposure ($P > 0.05$). (Fig. 5a,5b)

Control group and 40μmol/kg Al group were selected to detect the interaction of death key proteins by IP. Compared with the control group, the interaction between RIP1 and RIP3, RIP3 and MLKL, RIP3 and CaMKII enhanced in the Al-exposed group ($P < 0.05$). It clarified that the interaction between programmed necrosis-related protein RIP3 and RIP1, RIP3 and MLKL, RIP3 and CaMKII was strengthened in Al induced dementia-like models and proved that RIP3, RIP1, MLKL and CaMKII (precisely p-CaMK□) were all involved in the process of nerve cell death caused by aluminum. (Fig. 5c,5d)

In vivo study results

The necrosis rate

The necrosis rates of SH-SY5Y cells exposed to different doses of aluminum maltol for 24 hours were detected by flow cytometry. The necrosis rate of 100μM aluminum maltol treated cells was not statistically different from that of the control group after aluminum exposure for 24 hours ($P > 0.05$), while the necrosis rates in 200 and 400 μM aluminum maltol treated cells were significantly higher than that of the control group ($P < 0.05$), and, interestingly, the necrosis rate of 200μM aluminum maltol treated cells was the highest ($P < 0.05$), but, it was lowered in 400 μM aluminum maltol treated cells (Fig. 6).

Death related protein expression

The expression of RIP1, RIP3, and MLKL in 200μmol/L and 400μmol/L aluminum treated cells were higher than those in the control group ($P < 0.05$). The protein expressions of p-RIP3 and p-CaMKII of the cells began to increase in 100μmol/L aluminum concentration and reached the highest level in 200μmol/L aluminum concentration ($P < 0.05$). p-MLKL expressed the highest level in 200μmol/L aluminum treated cells ($P < 0.05$). Interestingly, p-RIP3, MLKL, and p-MLKL expressions of the cells began to decrease in 400μmol/L maltol aluminum concentration. The expression of CaMKII and ox-CaMKII did not change significantly after aluminum-treatment ($P > 0.05$) (Fig. 7).

GSK'872 administration on the necrosis rate, ROS and death-related protein expression of SH-SY5Y cells after aluminum exposure

Through preliminary experiments, it was found that after exposure to 200μM Al for 24 hours, the cell necrosis rate, amount of ROS, and the expression of death-related proteins were more obvious than other groups. Therefore, we chose 200μM aluminum maltol treated cells for intervention with GSK'872. The 200μmol/L Al resulted in higher cell necrosis rate than the control group ($P < 0.05$). After administration with GSK'872, the cell necrosis rate of 200μmol/L Al-exposed cells decreased, which was statistically different from the only 200μmol/L Al-exposed cells ($P < 0.05$) (Fig. 8a). After 200μM Al exposure, the amount of ROS in SH-SY5Y cells was higher than that in the control group ($P < 0.05$). Being similar, the amount of ROS decreased after GSK'872 intervention too, and the difference was statistically significant ($P < 0.05$). It expounded that GSK'872 can inhibit the generation of ROS induced by aluminum, and has a certain protective effect on damaged nerve cell (Fig. 8b).

After 200μM aluminum exposure, the protein expression of RIP1, RIP3, p-RIP3, MLKL, p-MLKL, and p-CaMKII significantly increased compared with the control group ($P < 0.05$), and the protein expression of CaMKII and ox-CaMKII was not statistically different ($P > 0.05$). After GSK'872 administration in Al-exposed cells, the protein expression of RIP3, p-RIP3, MLKL, p-MLKL, and p-CaMKII decreased compared with the only Al-exposed group ($P < 0.05$). There was no significant difference between the RIP1 and CaMKII protein expression after Al-exposure ($P > 0.05$) (Fig. 9c, 9d). The results indicated that GSK'872 could inhibit the expression of MLKL, p-MLKL and p-CaMKII, which indirectly indicated that MLKL and CaMKII were downstream molecules of RIP3. GSK'872 could inhibit phosphorylated CaMKII, but has no effect on ox-CaMKII. Perhaps in this experimental model, only phosphorylated CaMKII played a role.

On this basis, we further performed IP experiments to observe the interactions between these cell death-related key proteins. After 200μM aluminum maltol exposure, the interaction between RIP3 and RIP1, RIP3 and MLKL, RIP3 and CaMKII were all enhanced, and the difference was statistically significant compared with the control group ($P < 0.05$). After GSK'872 administration, the interaction between RIP3 and RIP1, RIP3 and MLKL, RIP3 and CaMKII all weakened, and the difference was statistically significant compared with 200μM Al group ($P < 0.05$) (Fig. 9e, 9f). It elucidated that both MLKL and CaMKII were downstream molecules of RIP3. After the intervention of GSK'872, the interaction between RIP3 and MLKL, RIP3 and CaMKII can be weakened, and the necrosis of nerve cells can be reduced, so to achieve the effect of protecting cells from damage of Al-exposure.

Effects of NSA and KN-93 on SH-SY5Y cells after aluminum exposure

After intervention on Al-exposed cells with NSA and KN-93, the necrosis rate of cells decreased significantly, which was statistically different from the aluminum-exposed but not intervened cells ($P < 0.05$)(Fig. 10a, 10b). It indicated that NSA and KN-93 could also inhibit cell necrosis caused by aluminum exposure, and played a significant protective role on nerve cells.

The amount of ROS in aluminum-exposed cells was reduced significantly by the intervention of NSA, a specific inhibitor of MLKL ($P < 0.05$) (Fig. 9c), indicating that NSA can inhibit the generation of ROS induced by aluminum, and has a certain protective effect on nerve cells. However, KN-93, a reversible inhibitor of CaMK-II, protected SH-SY5Y cells from aluminum induced cell necroptosis, and did not reduce the generation of ROS ($P > 0.05$) (Fig. 9d). Scholars had discovered that activation of protein CaMK-II could reduce the mitochondrial membrane potential to induce cell death. Our research team have previously proved that aluminum can cause the mitochondrial membrane potential decreasing. In present study, we tested the mitochondrial membrane potential of SH-SY5Y cells after aluminum exposure and intervened with KN-93. After 200μM Al exposure, the mitochondrial membrane potential in SH-SY5Y cells was lower than that in the control group ($P < 0.05$). The mitochondrial membrane potential after KN-93 intervention on Al-treated cells significantly increased compared with the only aluminum exposed group ($P < 0.05$) (Fig. 9e). It implies that KN-93 had a protective effect on neural cells by preventing from aluminum-induced mitochondrial membrane potential decrease. Inhibition of CaMK-II could prevent from

the mitochondrial membrane potential decreasing induced by aluminum exposure, thereby preventing cells from programmed necrosis.

GSK'872, NSA, KN-93 administration on the release of LDH after aluminum exposure

There was no difference in LDH release between the control group and the DMSO group, GSK'872 group, NSA group, and KN-93 group ($P > 0.05$). LDH release of nerve cells increased after aluminum exposure ($P < 0.05$). After GSK'872, NSA, KN-93 intervention, the LDH release of GSK'872 + Al, NSA + Al group, KN-93 + Al group decreased ($P < 0.05$)(Fig. 10).

Discussion

Our era belongs to the "Aluminum Era". Aluminum has applications in many areas of our daily lives, such as antacids, food additives, skin care products, cosmetics, cooking utensils, and vaccine adjuvants, etc(Dabeka et al., 2011; Tomljenovic & Shaw, 2011). Aluminum may also appear as an element or contaminant in many foods, including infant formula, dairy products, juice, wine, seafood, tea, etc(H. Cao, Qiao, Zhang, & Chen, 2010; Tariba, 2011). The way the human body takes in aluminum generally includes nasal inhalation of aluminum particles (Weinbruch et al., 2010) and gastrointestinal absorption(Krewski et al., 2007), and then enter the brain through the blood-brain barrier(Yokel, 2006). Various studies have confirmed that aluminum has been widely recognized as a certain nerve toxicant (Simonsen et al., 1994). The toxic effect of aluminum on the nervous system is suspected to be closely related to some neurodegenerative diseases such as Alzheimer's disease, amyotrophic lateral sclerosis, dialysis encephalopathy(Bondy, 2014). Aluminum is especially concentrated in the highly active neurons in the brain regions that are most vulnerable to damage in Alzheimer's disease(Yumoto et al., 2001), leading to abnormal structure and function of the corresponding brain regions, and then cognitive dysfunction and even dementia(Sakamoto, Ogasawara, Ishii, Takahashi, & Tanabe, 2004). In this experiment, the mice showed difficulty in spatial learning and memory in the Morris Water Maze, and presented impairment in short-term learning and memory in the new object recognition experiment, which was similar to the study of Li Huan(H. Li et al., 2020). The hippocampus is an important part of the memory system of the medial temporal lobe of the brain. It is mainly responsible for the coding and storage of information. The normal structure of the hippocampus is the anatomical basis for its normal function. Therefore, this study used histopathological specimens to observe the morphological structure of the hippocampus. After aluminum maltol treatment, the number of neurons in the CA1 and CA3 of the mouse hippocampus was reduced, and the cell arrangement was disordered. Nissl bodies reduced and the staining becomes lighter and uneven. Sandip T. had found that aluminum can reduce the number of hippocampal and cortical neurons(Auti & Kulkarni, 2019). A number of experiments have shown that aluminum can cause the reduction and disappearance of nerve cells in the brain, which is the structural basis of learning and memory impairment.

At present, the mechanism of the decrease and disappearance of nerve cells in neurodegenerative diseases was not fully understood, and programmed cell necrosis was suspected as one of the possible reasons. Studies have found that necroptosis was morphologically different from apoptosis. The typical morphology of necroptosis is the death feature of necrotic cells, including early plasma membrane permeability, organelle swelling, nuclear membrane expansion and chromatin agglutination(Vandenabeele et al., 2010). Eventually, the cell membrane ruptures and the cell contents are released, which often leads to inflammation(Ofengeim & Yuan, 2013). In this study, we observed the structure of subcellular organelles in the cell under electron microscope. After aluminum exposure, the neuronal cell body became smaller, and some cell membranes even showed unclear borders and then dissolved and broken. The nuclear membrane of the nucleus became blurred, uneven, and dissolved and broken. The chromatin in the nucleus increased, forming clumps and gathering to the edge. The volume of mitochondria in the cytoplasm enlarged, and the inner chamber swollen, which were different from the apoptosis. The previous in vivo experiments of our research group have confirmed that after the intervention of Nec-1, a specific inhibitor of necroptosis, the number of brain neurons in the intervention group was significantly greater than that of the aluminum-exposed group, which reversedly proved that aluminum exposure can lead to programmed necrosis of nerve cells(Hao et al., 2020).

The key proteins in the signaling pathway of programmed necrosis are receptor interacting protein 1 (RIP1) and interacting protein 3 (RIP3), the upstream of which is the tumor necrosis factor receptor family (TNFRs) and Toll-like receptor family sending the death signal. Studies have shown that RIP1 is involved in cell death in multiple organs and diseases, such as motor neuron cell death(Oppenheim et al., 2001), pancreatitis(Mareninova et al., 2006), Alzheimer's disease(Caccamo et al., 2017). Inhibition of RIP1 has an antagonistic effect on necroptosis (Degterev et al., 2008). The interaction between RIPK1 and RIPK3 to form a complex is necessary for programmed cell necrosis. After RIP1 activated, RIPK3 is phosphorylated, or RIP3 is autophosphorylated(Sun et al., 1999), and the activated RIP3 recruits downstream proteins to cause necroptosis. In the process of TNF-α induced cell necrosis, RIP3 forms a protein complex with RIP1, which is phosphorylated(D. W. Zhang et al., 2009). Further research found that when wild-type mice and RIP3 knockout mice were injected with TNF-α into the brain, the hippocampal CA3 of wild-type mice showed a decrease in neuron density in a dose-dependent manner, while RIP3 knockout mice did not show neuron density decrease. The phenomenon indicates that RIP3 is an indispensable factor for TNF-α to induce the hippocampal neurons necroptosis(D. W. Zhang et al., 2009). Our research team proved that TNFR1, RIPK1 and RIPK3 played important roles in the aluminum induced programmed necrosis of nerve cells. In this experiment, the expression of RIP1 and RIP3 increased after aluminum exposure, and the interaction of RIP1-RIP3 enhanced. After inhibiting the expression of RIPK3 with GSK'872, the PI stained programmed necrotic cells was less than that before the intervention, as well as the interaction of RIPK1-RIPK3 weakened, and the release of LDH was less than that of the aluminum-exposed cells without GSK'872 intervention. This experiment also discovered that inhibiting the expression of RIP3 with GSK'872 can reduce the generation of ROS. It was proved that the generation of ROS in Al-exposed neural cells is another major cause of memory impairment and accelerates cell death(Singla & Dhawan, 2013; Q. L. Zhang, Niu, Niu, & Wang, 2005). In this research, inhibiting the

expression of RIP3 not only reduce the cell death directly, but also lessen the generation of ROS indirectly, thus protect the nerve cell from necroptosis.

Mixed lineage linase domain like (MLKL), the substrate protein of RIP3 discovered by Wang(H. Wang et al., 2014), is a kind of pseudokinase, and only possesses a kinase domain but has no kinase function. In the initial stage of necrosome formation, threonine 227 of RIP3 is phosphorylated, which enables MLKL to bind to it. Only with the participation of MLKL can the necroptosis function be performed, otherwise the necroptosis complex will be stopped in the precursor stage. Threonine 375 and serine 358 of the kinase domain are phosphorylated by RIP3 when programmed cell death is initiated. After being activated by RIP3, MLKL transforms from a monomeric state to a multimeric state. It moves from the cytoplasm to the cell membrane, penetrating into the membrane bilayer, and then formes permeable pores in the cell membrane. At last, the cell membrane is destroyed, and cells are going to death(H. Wang et al., 2014). MLKL-deficient cells have the ability to resist the necroptosis, indicating that inhibiting MLKL can protect cells from programmed cell necrosis(Zhao et al., 2012). In vitro experiment, not only RIPK3 and MLKL increased, but also the phosphorylation at S227 of RIPK3 and Ser358 of MLKL increased after aluminum exposure. More importantly, the phosphorylation expression of Ser358 of MLKL was the highest when 200 μM aluminum was exposed for 24 hours, and the necrosis rate of PI stained cells was the highest. Therefore, we choose 200μM aluminum maltolate as a model exposure dose for following experiments. After GSK'872 intervention, the expressions of RIPK3 and MLKL were reduced, and the interaction of RIPK3-MLKL was lower than that of the aluminum exposure group. It demonstrates that MLKL activates in the aluminum-exposed cells and plays a role of necroptosis as a downstream molecule of RIPK3. In addition, we also used NSA, a specific inhibitor of MLKL, to intervene MLKL in the Al-exposed cell. The results show that NSA can effectively inhibit the necroptosis of Al-exposed cell. NSA significantly reduced the number of PI stained cells and LDH release. At the same time, NSA can reduce the generation of ROS in aluminum-exposed cells. It clarifies that inhibiting MLKL protein can reduce the generation of ROS and then reduce the occurrence of programmed necrosis.

Recently, CaMKII is reported as another substrate of RIPK3, which plays an important role in programmed cell death during myocardial ischemia(T. Zhang et al., 2016). CaMKII is activated by direct phosphorylation and indirect oxidation, which leads to the opening of mitochondrial nuclear membrane pores, and finally leads to cell death after the decrease of mitochondrial membrane potential(T. Zhang et al., 2016). In this in vivo and in vitro study, we discovered that p- CaMKII, not ox- CaMKII, play key role in Al-induced cell necroptosis, which is consistent with Yi Qu(Qu et al., 2017). After GSK'872 intervention, the expressions of RIPK3 and p- CaMKII were reduced, and the interaction of RIPK3- CaMKII was lower than that of the aluminum exposure group. It indicates that CaMKII activates in the aluminum-exposed cells and plays a role in necroptosis as a downstream molecule of RIPK3. In addition, we also used KN-93, an inhibitor of CaMKII, to intervene CaMKII in the Al-exposed cell. The results show that KN-93 can effectively inhibit the necroptosis of Al-exposed cell. The number of PI stained cells and LDH release decreased after administration of KN-93. At the same time, KN-93 could not reduce the generation of ROS in Al-exposed cells, but it can increase the mitochondrial membrane potential which was dropped in Al-exposed cells, and protect nerve cells from damage.

The survival or death of nerve cells, and the main way of death depends on the source, duration and dose of different stressors, as well as cell types and metabolic conditions. In vivo and in vitro experiments, we have proved that RIP1, RIP3, MLKL and CaMKII exert programmed cell necrosis and play important roles in aluminum-induced neuronal cell death. The critical pathway of death is mediated by both RIP1-RIP3-MLKL and RIP1-RIP3-CaMK□. That is, there is one initiating molecule – RIP1, are two downstream signaling pathways : RIP3-MLKL and RIP3-CaMK□. The present study will provide a scientific basis for further clarification of mechanism and the possible intervention for aluminum-induced cognitive impairment.

Declarations

Acknowledgement This study was supported by the Natural Science Foundation of China (NSFC, 81430078).

Compliance with Ethical Standards

Conflict of Interest The authors declare that there are no conflicts of interest.

References

1. Auti, S. T., & Kulkarni, Y. A. (2019). Neuroprotective Effect of Cardamom Oil Against Aluminum Induced Neurotoxicity in Rats. Front Neurol, *10*, 399. doi: 10.3389/fneur.2019.00399
2. Bondy, S. C. (2010). The neurotoxicity of environmental aluminum is still an issue. Neurotoxicology, *31*(5), 575–581. doi: 10.1016/j.neuro.2010.05.009
3. Bondy, S. C. (2014). Prolonged exposure to low levels of aluminum leads to changes associated with brain aging and neurodegeneration. Toxicology, *315*, 1–7. doi: 10.1016/j.tox.2013.10.008
4. Caccamo, A., Branca, C., Piras, I. S., Ferreira, E., Huentelman, M. J., Liang, W. S.,.. . Oddo, S. (2017). Necroptosis activation in Alzheimer's disease. Nat Neurosci, *20*(9), 1236–1246. doi: 10.1038/nn.4608
5. Cao, H., Qiao, L., Zhang, H., & Chen, J. (2010). Exposure and risk assessment for aluminium and heavy metals in Puerh tea. Sci Total Environ, *408*(14), 2777–2784. doi: 10.1016/j.scitotenv.2010.03.019
6. Cao, Z., Yang, X., Zhang, H., Wang, H., Huang, W., Xu, F.,.. . Li, Y. (2016). Aluminum chloride induces neuroinflammation, loss of neuronal dendritic spine and cognition impairment in developing rat. Chemosphere, *151*, 289–295. doi: 10.1016/j.chemosphere.2016.02.092
7. Dabeka, R., Fouquet, A., Belisle, S., & Turcotte, S. (2011). Lead, cadmium and aluminum in Canadian infant formulae, oral electrolytes and glucose solutions. Food Additives & Contaminants: Part A, *28*(6), 744–753. doi: 10.1080/19393210.2011.571795
8. Degterev, A., Hitomi, J., Germscheid, M., Ch'en, I. L., Korkina, O., Teng, X.,.. . Yuan, J. (2008). Identification of RIP1 kinase as a specific cellular target of necrostatins. Nat Chem Biol, *4*(5), 313–

321. doi: 10.1038/nchembio.83

9. Degterev, A., Huang, Z., Boyce, M., Li, Y., Jagtap, P., Mizushima, N.,.. . Yuan, J. (2005). Chemical inhibitor of nonapoptotic cell death with therapeutic potential for ischemic brain injury. Nat Chem Biol, *1*(2), 112–119. doi: 10.1038/nchembio711
10. Edwardson, J. A., Candy, J. M., Ince, P. G., McArthur, F. K., Morris, C. M., Oakley, A. E.,.. . Bjertness, E. (1992). Aluminium accumulation, beta-amyloid deposition and neurofibrillary changes in the central nervous system. *Ciba Found Symp, 169*, 165–179; discussion 179–185. doi: 10.1002/9780470514306.ch10
11. Foyet, H. S., & Keugong Wado, E. (2019). Anticholinesterase and Antioxidant Potential of Hydromethanolic Extract of Ziziphus mucronata (Rhamnaceae) Leaves on Scopolamine-Induced Memory and Cognitive Dysfunctions in Mice. *2019*, 4568401. doi: 10.1155/2019/4568401
12. Han, S., Lemire, J., Appanna, V. P., Auger, C., Castonguay, Z., & Appanna, V. D. (2013). How aluminum, an intracellular ROS generator promotes hepatic and neurological diseases: the metabolic tale. Cell Biol Toxicol, *29*(2), 75–84. doi: 10.1007/s10565-013-9239-0
13. Hanninen, H., Matikainen, E., Kovala, T., Valkonen, S., & Riihimaki, V. (1994). Internal load of aluminum and the central nervous system function of aluminum welders. Scandinavian Journal of Work, Environment & Health, *20*(4), 279–285. doi: 10.5271/sjweh.1397
14. Hao, Y. X., Li, M. Q., Zhang, J. S., Zhang, Q. L., Jiao, X., Ji, X. L.,.. . Niu, Q. (2020). Aluminum-induced "mixed" cell death in mice cerebral tissue and potential intervention. *37*(4), 835–846. doi: 10.1007/s12640-019-00123-w
15. Ishida, A., Shigeri, Y., Taniguchi, T., & Kameshita, I. (2003). Protein phosphatases that regulate multifunctional Ca2+/calmodulin-dependent protein kinases: from biochemistry to pharmacology. Pharmacology & Therapeutics, *100*(3), 291–305. doi: 10.1016/j.pharmthera.2003.09.003
16. Kawahara, M., & Kato-Negishi, M. (2011). Link between Aluminum and the Pathogenesis of Alzheimer's Disease: The Integration of the Aluminum and Amyloid Cascade Hypotheses. *Int J Alzheimers Dis, 2011*, 276393. doi: 10.4061/2011/276393
17. Krewski, D., Yokel, R. A., Nieboer, E., Borchelt, D., Cohen, J., Harry, J.,.. . Rondeau, V. (2007). Human health risk assessment for aluminium, aluminium oxide, and aluminium hydroxide. J Toxicol Environ Health B Crit Rev, *10 Suppl 1*(Suppl 1), 1–269. doi: 10.1080/10937400701597766
18. Leger, M., Quiedeville, A., Bouet, V., Haelewyn, B., Boulouard, M., Schumann-Bard, P., & Freret, T. (2013). Object recognition test in mice. Nat Protoc, *8*(12), 2531–2537. doi: 10.1038/nprot.2013.155
19. Li, H., Xue, X., Li, L., Li, Y., Wang, Y., Huang, T.,.. . Niu, Q. (2020). Aluminum-Induced Synaptic Plasticity Impairment via PI3K-Akt-mTOR Signaling Pathway. Neurotox Res, *37*(4), 996–1008. doi: 10.1007/s12640-020-00165-5
20. Li, J., McQuade, T., Siemer, A. B., Napetschnig, J., Moriwaki, K., Hsiao, Y. S.,.. . Wu, H. (2012). The RIP1/RIP3 necrosome forms a functional amyloid signaling complex required for programmed necrosis. Cell, *150*(2), 339–350. doi: 10.1016/j.cell.2012.06.019

21. Liang, R. F., Li, W. Q., Wang, X. H., Zhang, H. F., Wang, H., Wang, J. X.,.. . Niu, Q. (2012). Aluminium-maltolate-induced impairment of learning, memory and hippocampal long-term potentiation in rats. Ind Health, *50*(5), 428–436. doi: 10.2486/indhealth.ms1330
22. Mareninova, O. A., Sung, K. F., Hong, P., Lugea, A., Pandol, S. J., Gukovsky, I., & Gukovskaya, A. S. (2006). Cell death in pancreatitis: caspases protect from necrotizing pancreatitis. J Biol Chem, *281*(6), 3370–3381. doi: 10.1074/jbc.M511276200
23. Meyer-Baron, M., Sch 10.1074/jbc.M511276200van Thriel, C. (2007). Occupational aluminum exposure: evidence in support of its neurobehavioral impact. *Neurotoxicology, 28*(6), 1068–1078. doi: 10.1016/j.neuro.2007.07.001
24. Nie, J. (2018). Exposure to Aluminum in Daily Life and Alzheimer's Disease. Adv Exp Med Biol, *1091*, 99–111. doi: 10.1007/978-981-13-1370-7_6
25. Nie, J., Lv, S., Fu, X., & Niu, Q. (2019). Effects of Al Exposure on Mitochondrial Dynamics in Rat Hippocampus. Neurotox Res, *36*(2), 334–346. doi: 10.1007/s12640-019-00045-7
26. Ofengeim, D., & Yuan, J. (2013). Regulation of RIP1 kinase signalling at the crossroads of inflammation and cell death. Nature Reviews Molecular Cell Biology, *14*(11), 727–736. doi: 10.1038/nrm3683
27. Oppenheim, R. W., Flavell, R. A., Vinsant, S., Prevette, D., Kuan, C. Y., & Rakic, P. (2001). Programmed cell death of developing mammalian neurons after genetic deletion of caspases. J Neurosci, *21*(13), 4752–4760. doi: 10.1523/jneurosci.21-13-04752.2001
28. Prakash, A., & Kumar, A. (2013). Mitoprotective effect of Centella asiatica against aluminum-induced neurotoxicity in rats: possible relevance to its anti-oxidant and anti-apoptosis mechanism. Neurol Sci, *34*(8), 1403–1409. doi: 10.1007/s10072-012-1252-1
29. Qinli, Z., Meiqing, L., Xia, J., Li, X., Weili, G., Xiuliang, J.,.. . Qiao, N. (2013). Necrostatin-1 inhibits the degeneration of neural cells induced by aluminum exposure. Restorative neurology and neuroscience, *31*(5), 543–555. doi: 10.3233/rnn-120304
30. Qu, Y., Tang, J., Wang, H., Li, S., Zhao, F., Zhang, L.,.. . Mu, D. (2017). RIPK3 interactions with MLKL and CaMKII mediate oligodendrocytes death in the developing brain. Cell Death Dis, *8*(2), e2629. doi: 10.1038/cddis.2017.54
31. Russ, T. C., Killin, L. O. J., Hannah, J., Batty, G. D., Deary, I. J., & Starr, J. M. (2019). Aluminium and fluoride in drinking water in relation to later dementia risk. The British Journal of Psychiatry, *216*(1), 29–34. doi: 10.1192/bjp.2018.287
32. Sakamoto, T., Ogasawara, Y., Ishii, K., Takahashi, H., & Tanabe, S. (2004). Accumulation of aluminum in ferritin isolated from rat brain. Neurosci Lett, *366*(3), 264–267. doi: 10.1016/j.neulet.2004.05.045
33. Simonsen, L., Johnsen, H., Lund, S. P., Matikainen, E., Midtgbe, S. (2004). Accumulation of aluminum in ferritin isolated from rat brn of neurotoxicity data and the classification of neurotoxic chemicals. Scand J Work Environ Health, *20*(1), 1–12. doi: 10.5271/sjweh.1435
34. Singla, N., & Dhawan, D. K. (2013). Zinc protection against aluminium induced altered lipid profile and membrane integrity. Food Chem Toxicol, *55*, 18–28. doi: 10.1016/j.fct.2012.12.047

35. Song, J., Liu, Y., Zhang, H. F., & Niu, Q. (2016). The RAS/PI3K Pathway is Involved in the Impairment of Long-term Potentiation Induced by Acute Aluminum Treatment in Rats. Biomed Environ Sci, *29*(11), 782–789. doi: 10.3967/bes2016.105

36. Sun, X., Lee, J., Navas, T., Baldwin, D. T., Stewart, T. A., & Dixit, V. M. (1999). RIP3, a novel apoptosis-inducing kinase. J Biol Chem, *274*(24), 16871–16875. doi: 10.1074/jbc.274.24.16871

37. Tariba, B. (2011). Metals in wine–impact on wine quality and health outcomes. Biol Trace Elem Res, *144*(1–3), 143–156. doi: 10.1007/s12011-011-9052-7

38. Tomljenovic, L., & Shaw, C. A. (2011). Aluminum vaccine adjuvants: are they safe? Curr Med Chem, *18*(17), 2630–2637. doi: 10.2174/092986711795933740

39. Vandenabeele, P., Galluzzi, L., Vanden Berghe, T., & Kroemer, G. (2010). Molecular mechanisms of necroptosis: an ordered cellular explosion. Nat Rev Mol Cell Biol, *11*(10), 700–714. doi: 10.1038/nrm2970

40. Wang, H., Sun, L., Su, L., Rizo, J., Liu, L., Wang, L. F.,.. . Wang, X. (2014). Mixed lineage kinase domain-like protein MLKL causes necrotic membrane disruption upon phosphorylation by RIP3. Mol Cell, *54*(1), 133–146. doi: 10.1016/j.molcel.2014.03.003

41. Wang, S., Meng, H., Shang, N., Guo, J., Zhang, T., Zhang, S.,.. . Niu, Q. (2020). The Relationship between Plasma Al Levels and Multi-domain Cognitive Performance among In-service Aluminum-exposed Workers at the SH Aluminum Factory in China: A Cross-sectional Study. Neurotoxicology, *76*, 144–152. doi: 10.1016/j.neuro.2019.10.011

42. Weinbruch, S., Benker, N., Koch, W., Ebert, M., Drablang, S.,.. . Niu, Q. (2020)... Thomassen, Y. (2010). Hygroscopic properties of the workroom aerosol in aluminium smelter potrooms: a case for transport of HF and SO2 into the lower airways. *J Environ Monit, 12*(2), 448–454. doi: 10.1039/b919142a

43. Yokel, R. A. (2006). Blood-brain barrier flux of aluminum, manganese, iron and other metals suspected to contribute to metal-induced neurodegeneration. Journal of Alzheimer's disease: JAD, *10*(2–3), 223–253. doi: 10.3233/jad-2006-102-309

44. Yumoto, S., Nagai, H., Matsuzaki, H., Matsumura, H., Tada, W., Nagatsuma, E., & Kobayashi, K. (2001). Aluminium incorporation into the brain of rat fetuses and sucklings. Brain Res Bull, *55*(2), 229–234. doi: 10.1016/s0361-9230(01)00509-3

45. Zhang, D. W., Shao, J., Lin, J., Zhang, N., Lu, B. J., Lin, S. C.,.. . Han, J. (2009). RIP3, an energy metabolism regulator that switches TNF-induced cell death from apoptosis to necrosis. Science, *325*(5938), 332–336. doi: 10.1126/science.1172308

46. Zhang, Q. L., Niu, P. Y., Niu, Q., & Wang, L. P. (2005). Effect of aluminum on neuronal mitochondria of rats. Wei Sheng Yan Jiu, *34*(6), 674–677.

47. Zhang, T., Zhang, Y., & Cui, M. (2016). CaMKII is a RIP3 substrate mediating ischemia- and oxidative stress-induced myocardial necroptosis. *22*(2), 175–182. doi: 10.1038/nm.4017

48. Zhao, J., Jitkaew, S., Cai, Z., Choksi, S., Li, Q., Luo, J., & Liu, Z. G. (2012). Mixed lineage kinase domain-like is a key receptor interacting protein 3 downstream component of TNF-induced necrosis. Proc Natl Acad Sci U S A, *109*(14), 5322–5327. doi: 10.1073/pnas.1200012109

Figures

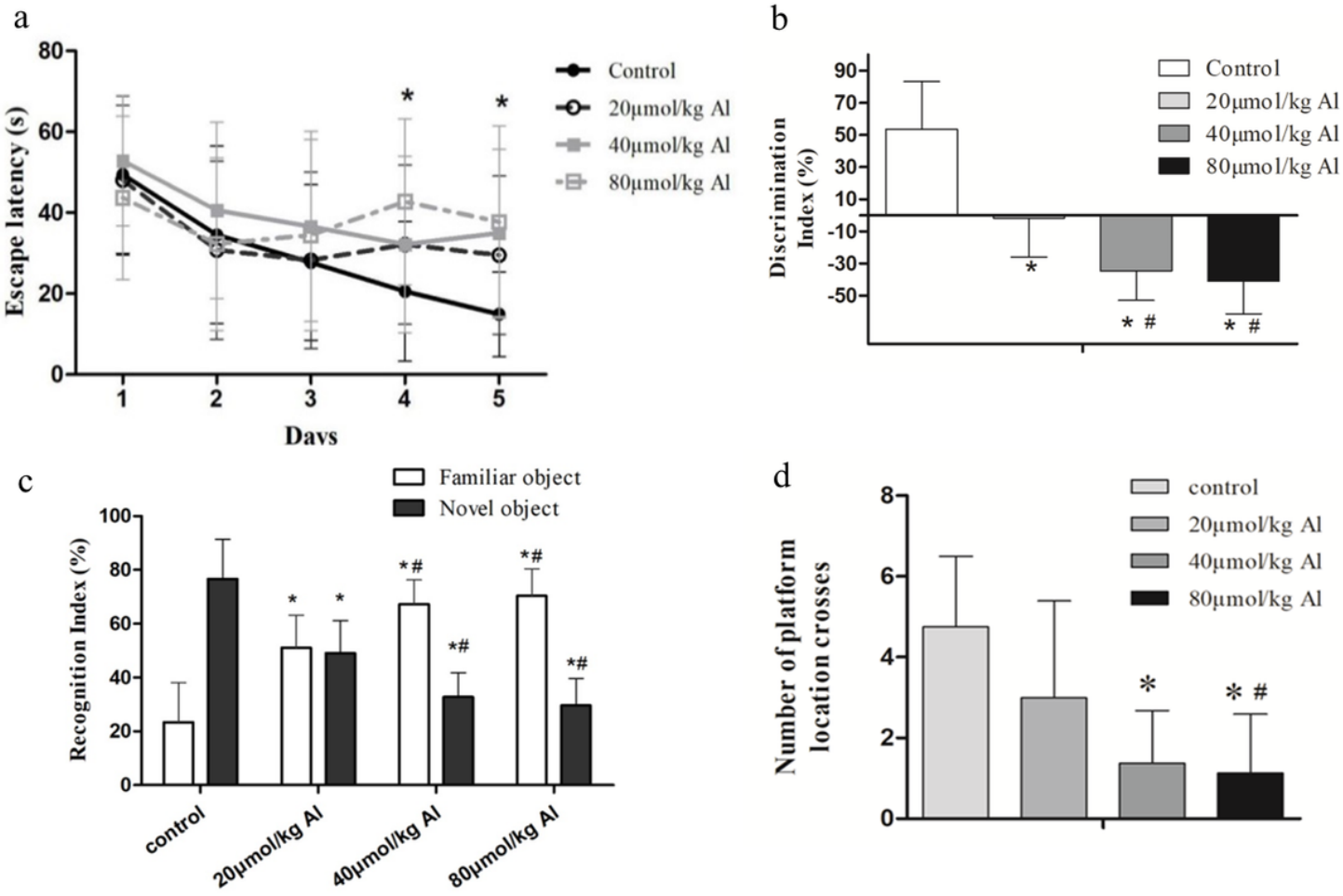

Figure 1

The results of Morris water maze Test and Object recognition test treated with different concentrations of Al $(mal)_3$. (a) Escape latency of mice exposed to Al $(mal)_3$ intraperitoneal injection with different doses. (b) The number of platform location crossed by different Al $(mal)_3$ exposed group. Values were represented as mean ± SD (n = 8). The results of Object recognition test treated with different concentrations of Al $(mal)_3$. (c) New object recognition index of mice after exposure to different concentrations of aluminum maltol. (d) New Object Discrimination Index in Mice after subchronic aluminum exposure. Values were represented as mean ± SD (n = 8). Compared with the control group, $^{*}P < 0.05$; compared with the 20 μmol/kg Al$(mal)_3$ group,$^{\#}$ $P< 0.05$; compared with the 40 μmol/kg Al$(mal)_3$ group, $^{\&}P < 0.05$.

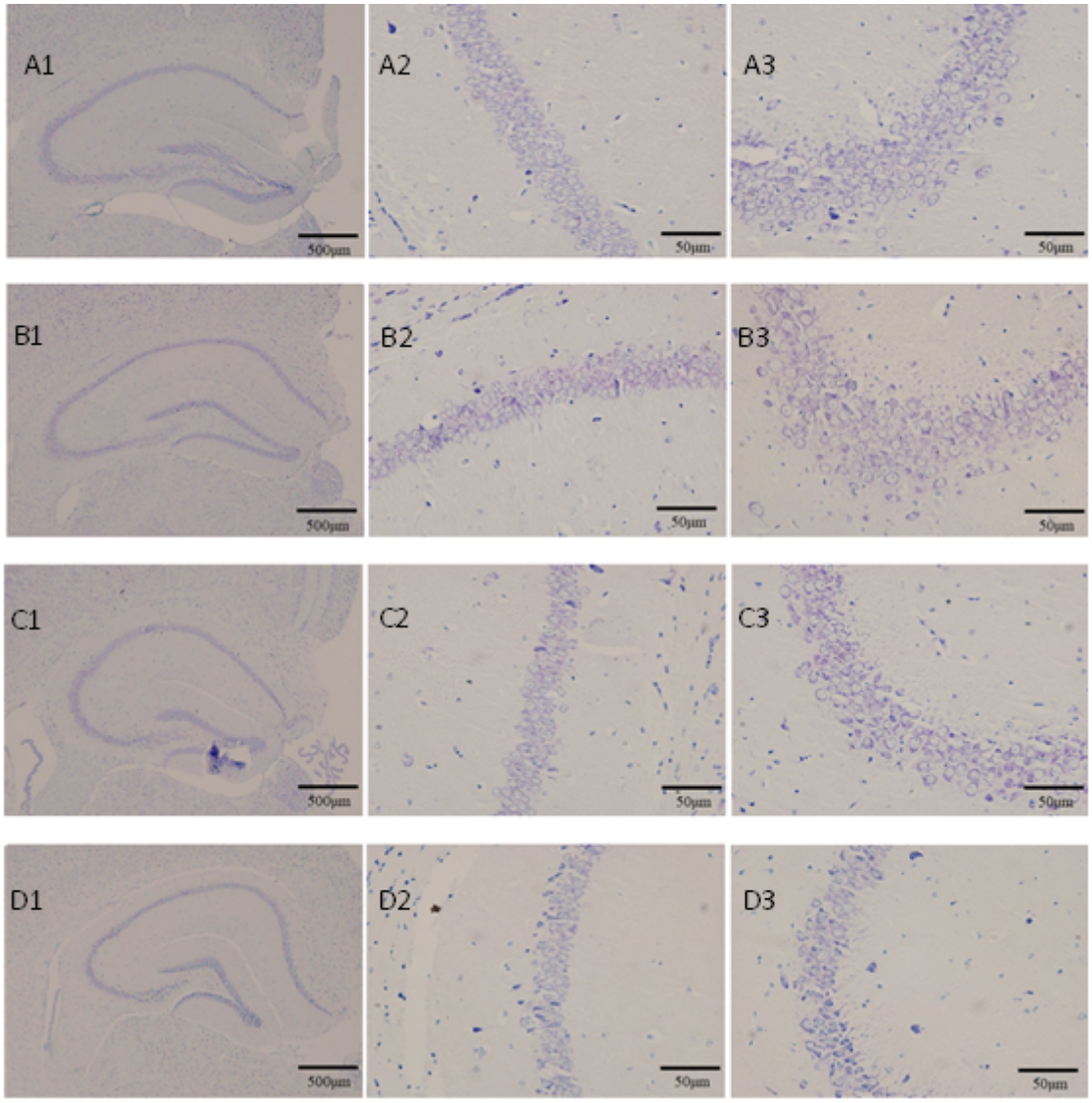

Figure 2

Images of Nussle stained mouse hippocampus after subchronic exposure to aluminum maltolate observed under microscope. A: Saline control group; B: 20μmol/kg Al exposure group; C: 40μmol/kg Al exposure group; D: 80μmol/kg Al exposure group.

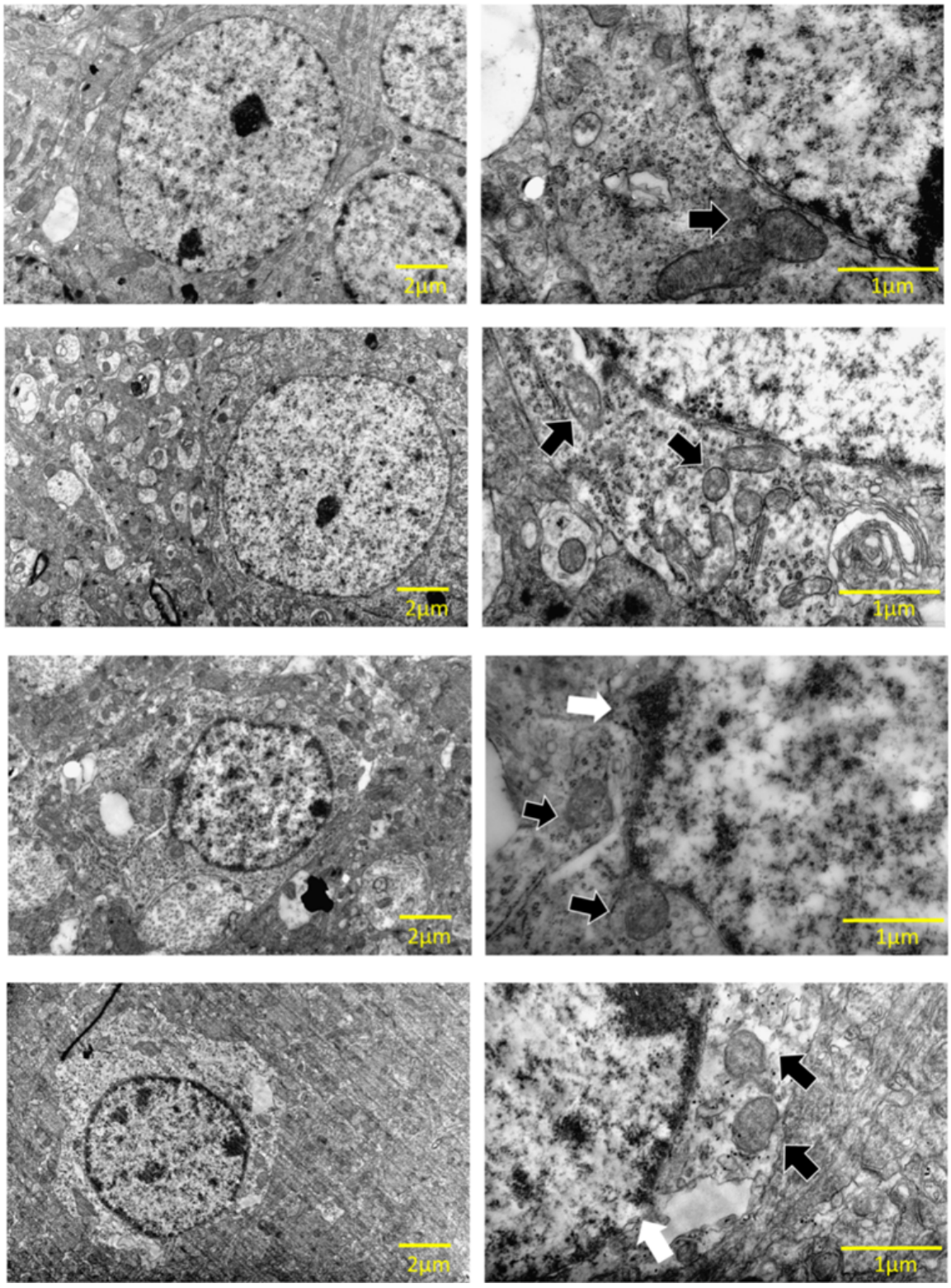

Figure 3

Electron micrograph of ultrastructure of mouse hippocampus was observed after subchronic exposure to Al. A: Saline control group; B: 20μmol/kg Al exposure group; C: 40μmol/kg Al exposure group; D: 80μmol/kg Al exposure group, left 1 picture is 10000× under microscope, right 2 picture is 40,000× Under the mirror. The white arrows indicate the rupture and disintegration of the nuclear membrane, and the black arrows indicate the mitochondria in each group.

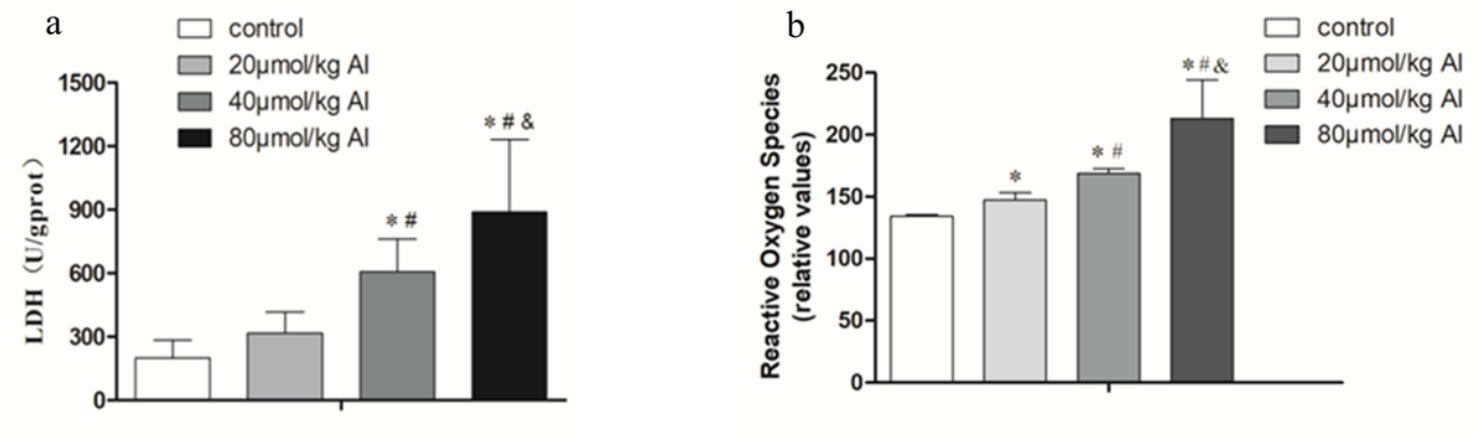

Figure 4

(a)The results of LDH Release treated with different concentrations of Al $(mal)_3$(b) ROS in the brain tissue exposed to different doses of intraperitoneal Al injection New Object Discrimination Index in Mice after Subchronic Aluminum Exposure. Values were represented as mean ± SD (n = 6). Compared with the control group, $^{*}P < 0.05$; compared with the 20 μmol/kg Al$(mal)_3$ group,$^{\#}$ $P< 0.05$; compared with the 40 μmol/kg Al$(mal)_3$ group, $^{\&}P < 0.05$.

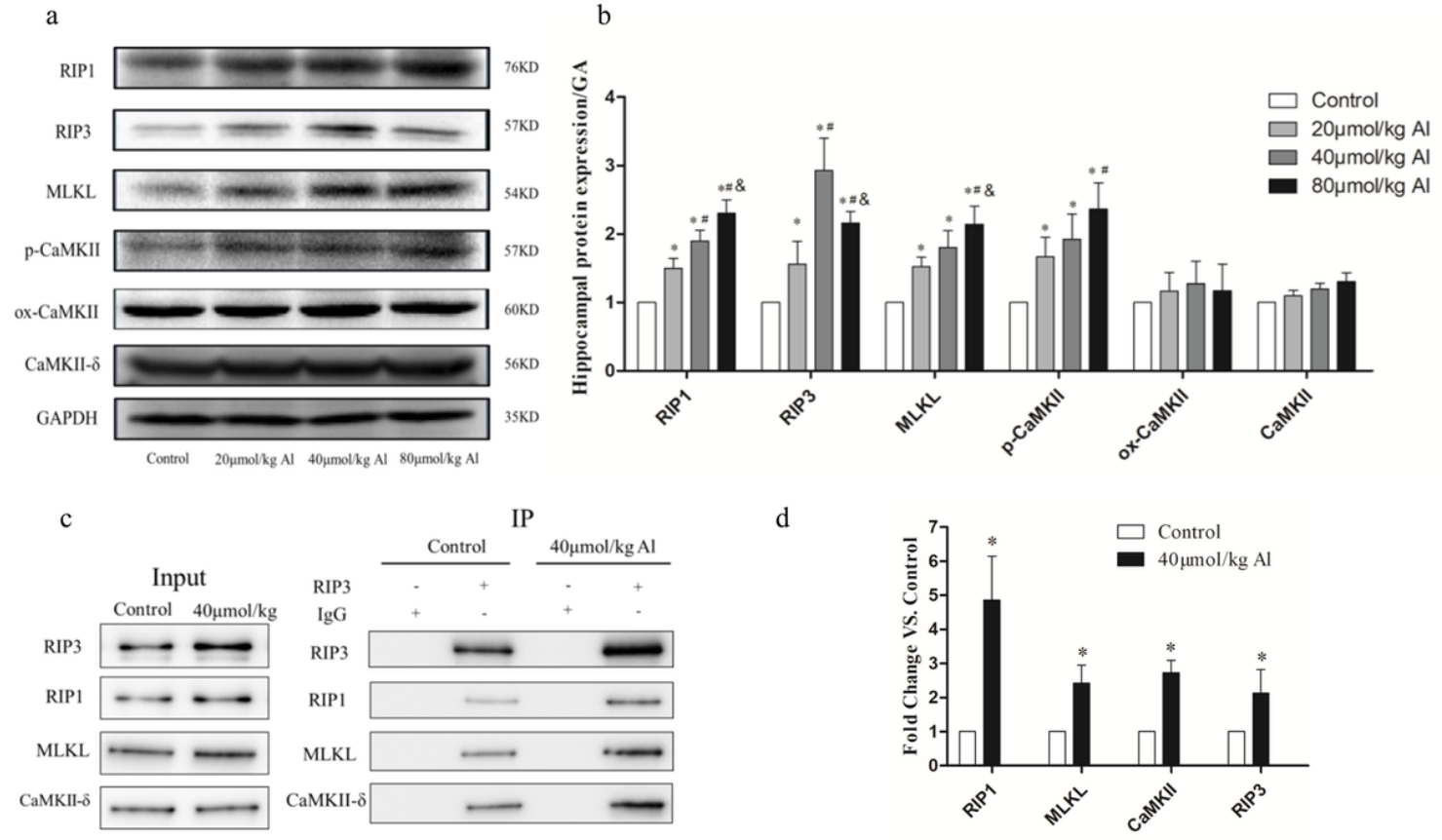

Figure 5

Expression of death-related proteins in hippocampal tissues of mice exposed to different doses of intraperitoneal Al injection. Hippocampal RIP1, RIP3, MLKL, CaMK□, p-CaMK□, ox-CaMK□ protein expression levels in mice of different dose groups by Western blot (a). Each column represents the mean ± SD (n = 6) of protein gray value (b). The interactions of RIP1 and RIP3, RIP3 and MLKL, and RIP3 and CaMKII in mouse cortex were detected by IP (c). Each column represents the mean ± SD (n = 6) of protein gray value (d). Compared with the control group, $^{*}P < 0.05$; compared with the 20 μmol/kg Al group, $^{\#}P < 0.05$. Compared with the 40 μmol/kg Al group, $^{\&}P < 0.05$.

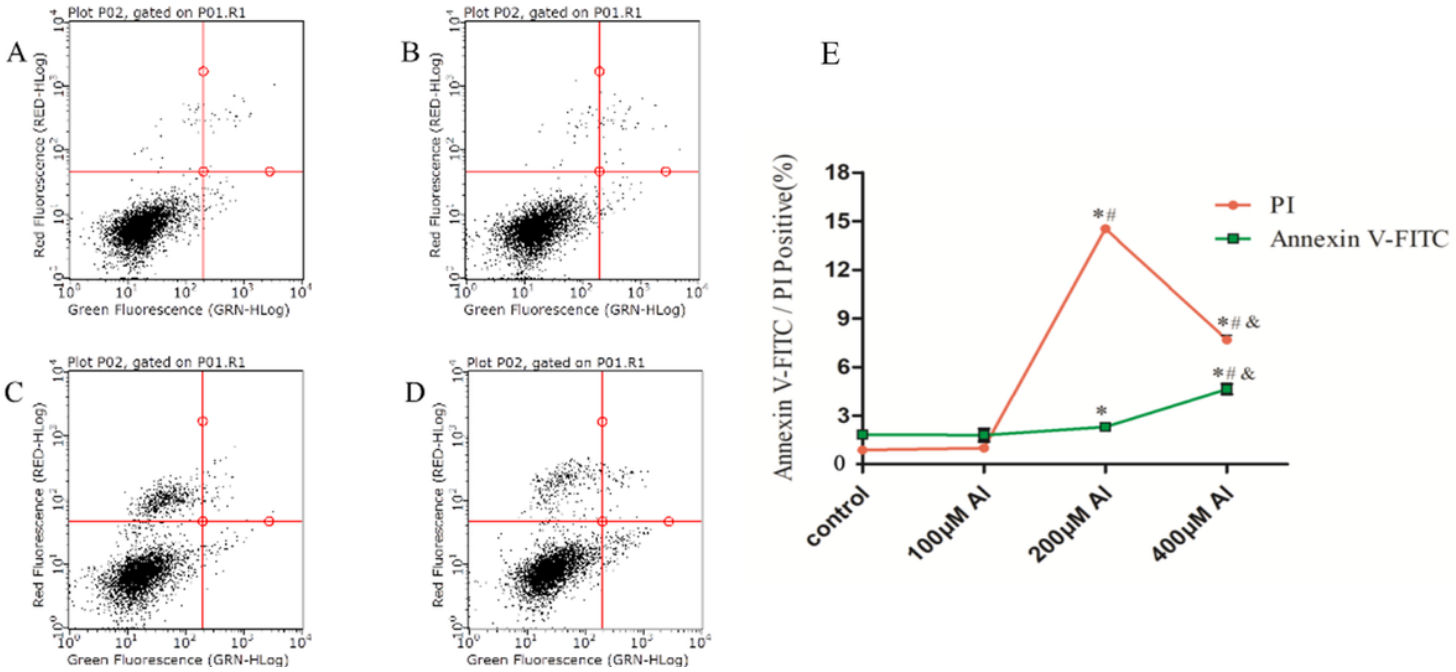

Figure 6

The necrosis rate of SH-SY5Y cells exposed to different doses of aluminum maltol for 24 hours was detected by flow cytometry. Picture A is the control group, Picture B is the 100 μmol/L Al group, Picture C is the 200 μmol/L Al group, and Picture D is the 400 μmol/L Al group. The red line graph in picture E presents cell necrosis after Al-exposed. Compared with the control group, $^{*}P < 0.05$; compared with the 200 μM Al group, $^{\#}P < 0.05$. Compared with the 400 μM Al group, $^{\&}P < 0.05$.

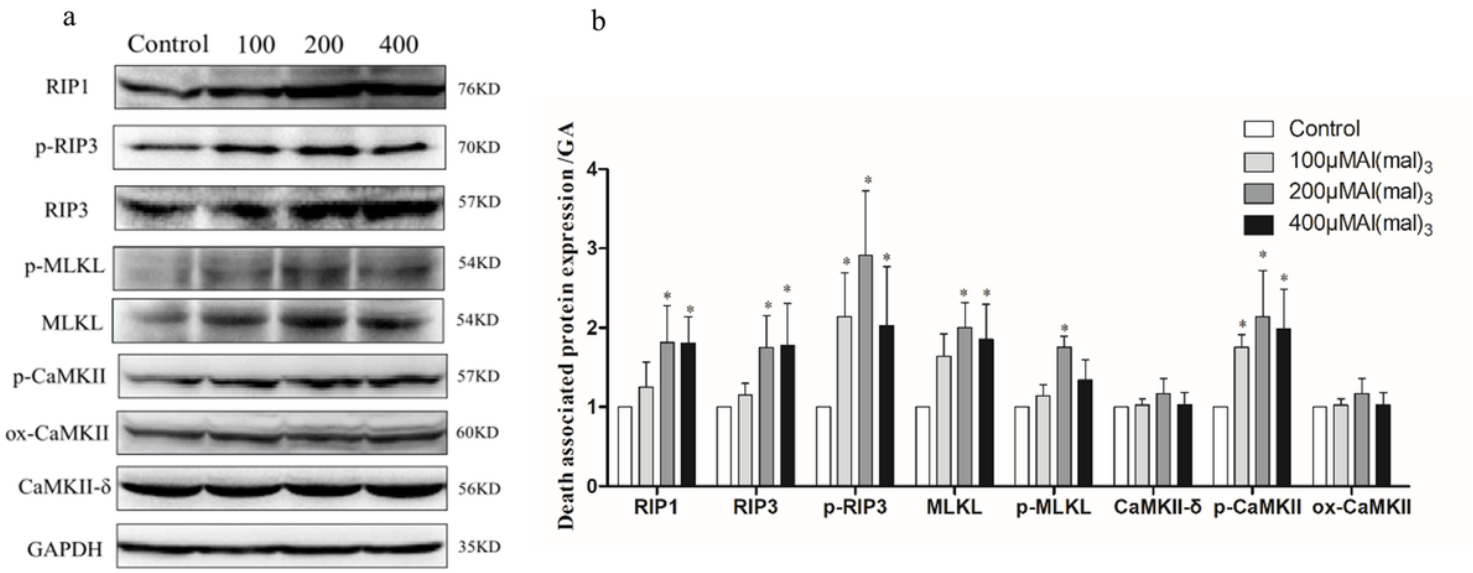

Figure 7

Expression of death-related proteins of the cells in different concentrations of aluminum maltol exposure for 24 hours. RIP1, RIP3, p-RIP3, MLKL, p-MLKL, CaMK□, p-CaMK□, ox-CaMK□ protein expression in SH-SY5Y exposed to different dose Al by Western blot (a). Each column represents the mean ± SD of protein gray value (b). Compared with the control group, $^{*}P < 0.05$.

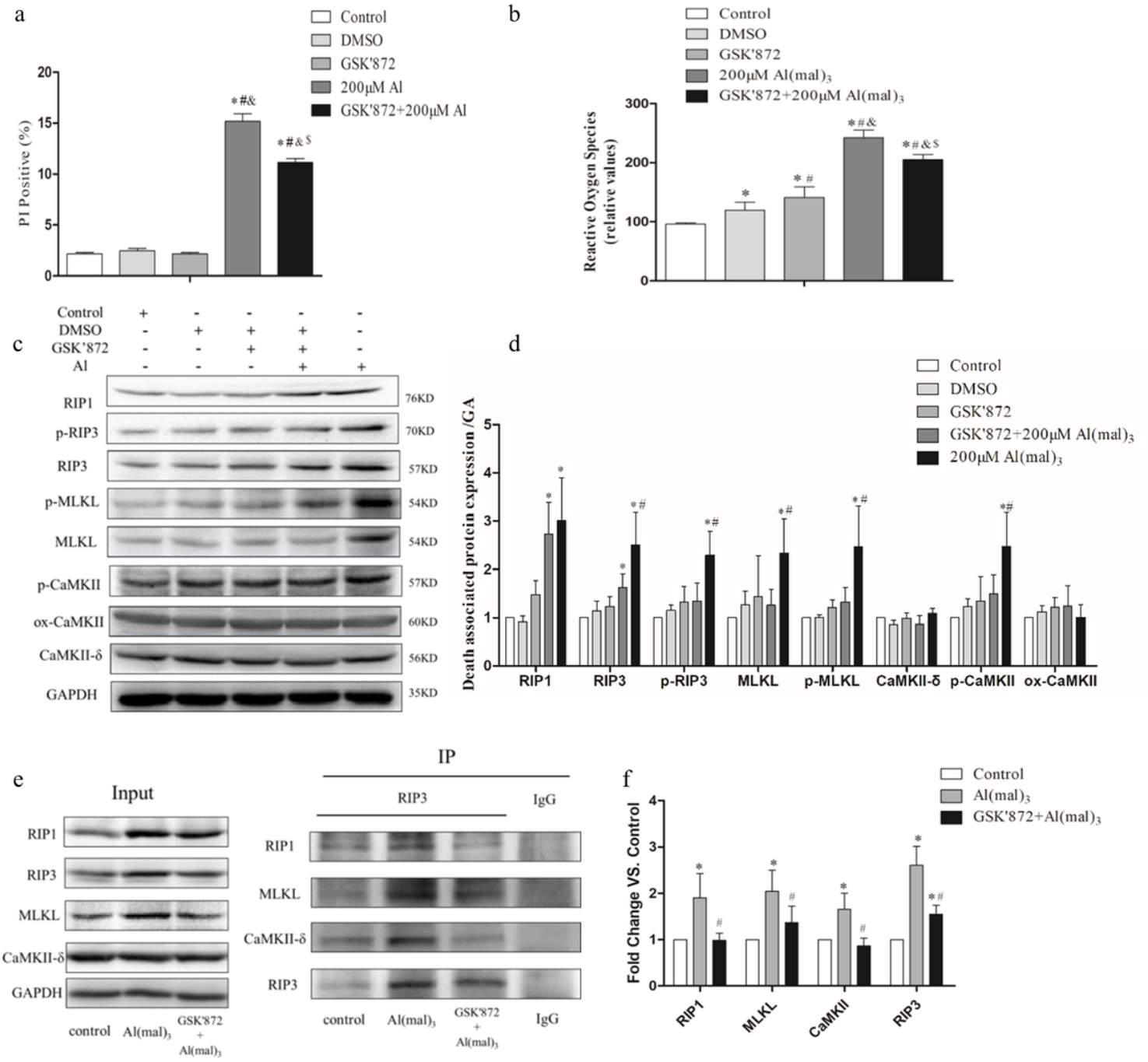

Figure 8

(**a**) GSK'872 administration on the necrosis rate of SH-SY5Y cells after aluminum exposure. GSK'872=5μmol/L. (**b**) GSK'872 administration on the ROS of SH-SY5Y cells after aluminum exposure. Each column represents the mean ± SD of protein gray value. Compared with the control group, $^{*}P < 0.05$; compared with the DMSO group, $^{\#}P < 0.05$. Compared with GSK'872 group, $^{\&}P < 0.05$; Compared with GSK'872+Al group, $^{\$}P < 0.05$. (**c, d**) Result of RIP1, RIP3, p-RIP3, MLKL, p-MLKL, p-CaMKII, CaMKII and ox-CaMKII expression in Al-exposed cell treated with GSK'872 administration. Compared with the control group, $^{*}P < 0.05$; compared with the GSK'872+Al group, $^{\#}P < 0.05$. (**e, f**) After 200μM Al exposure, the

interaction between RIP3 and RIP1, RIP3 and MLKL, RIP3 and CaMKII was tested by IP. Compared with the control group, $^{*}P < 0.05$; compared with the 200μM Al group, $^{\#}P < 0.05$.

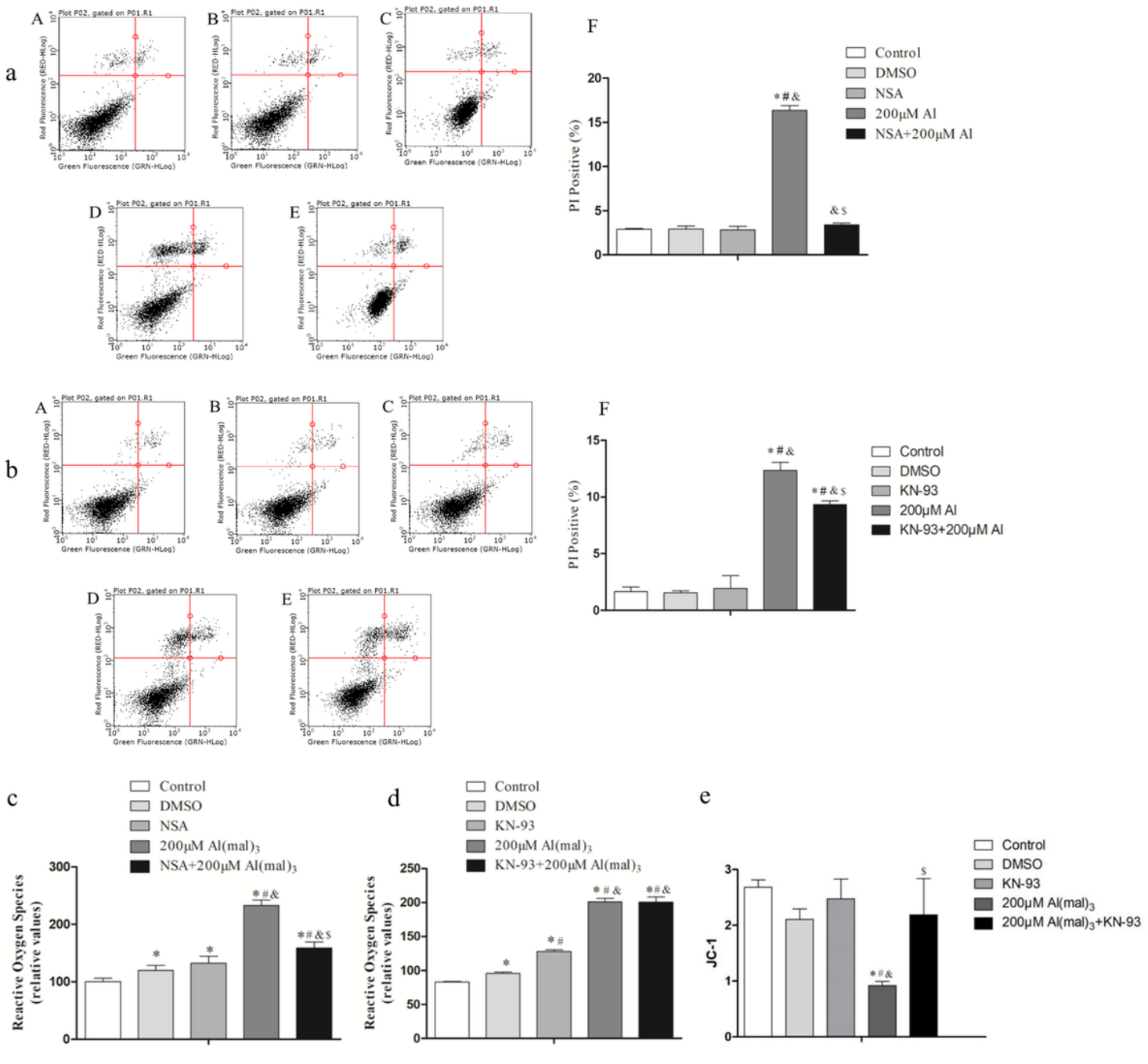

Figure 9

(**a**) The effect of NSA on the mortality of SH-SY5Y cells after aluminum exposure. NSA =10μmol/L A: the control group, B: the DMSO group, C: the NSA group, D: the 200 μM Al group, E: the NSA +200 μM Al group. F: Each column represents the mean ± SD of protein gray value. (**c**) The effect of NSA on ROS of SH-SY5Y cells after aluminum exposure. Compared with the control group, $^{*}P < 0.05$; compared with the DMSO group, $^{\#}P < 0.05$. Compared with NSA group, $^{\&}P < 0.05$; Compared with Al group, $^{\$}P < 0.05$. (**b**) The effect of KN-93 on the mortality of SH-SY5Y cells after aluminum exposure. KN-93=5μmol/L. A: the

control group, B: the DMSO group, C: the KN-93 group, D: the 200 μM Al group, E: the KN-93 +200 μM Al group. F: Each column represents the mean ± SD of protein gray value. (**d**) The effect of KN-93 on ROS of SH-SY5Y cells after aluminum exposure. (**e**) The effect of KN-93 on mitochondrial membrane potential of SH-SY5Y cells after aluminum exposure. Compared with the control group, $^{*}P < 0.05$; compared with the DMSO group, $^{\#}P < 0.05$. Compared with KN-93 group, $^{\&}P < 0.05$; Compared with Al group, $^{\$}P < 0.05$.

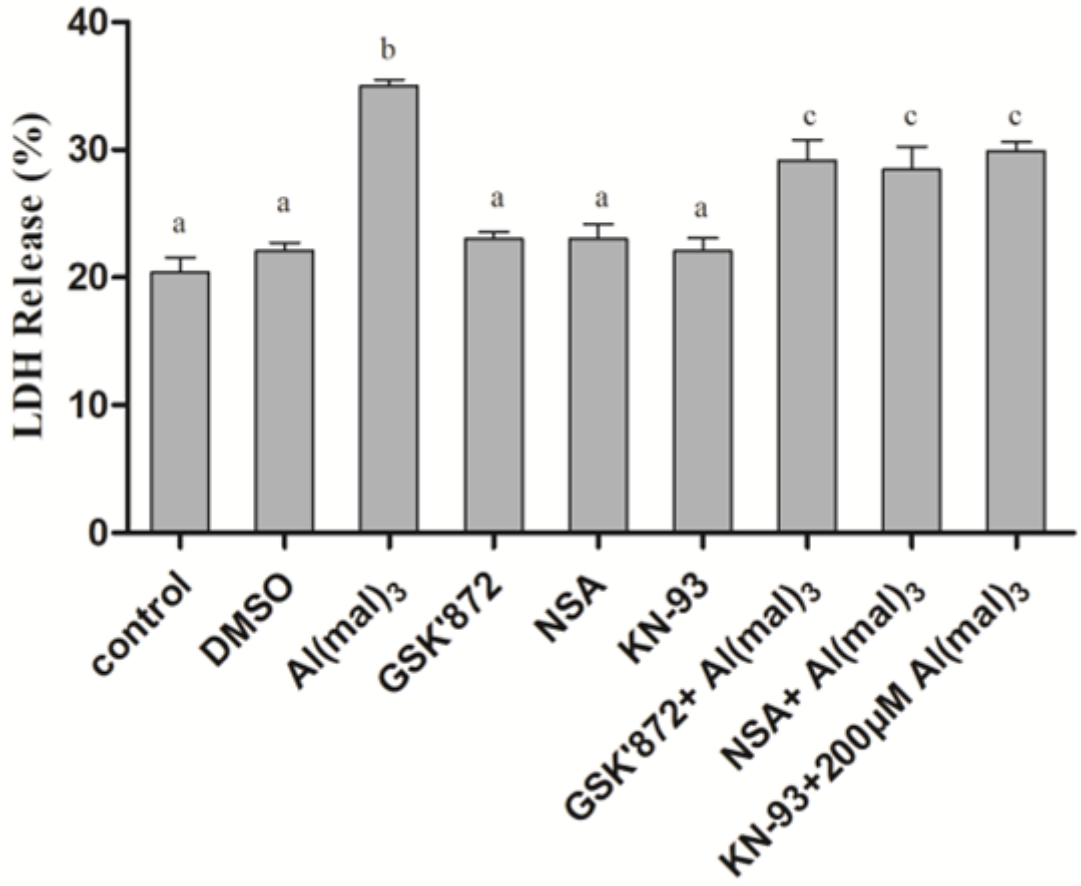

Figure 10

LDH released after inhibitor intervention in Al-exposed cells. Different letters mean that the difference is statistically significant, *P < 0.05.

Supplementary Files

This is a list of supplementary files associated with this preprint. Click to download.

- WBoriginalpicture.rar